Microstructural Evolution and Mechanical Properties of Simulated Heat-Affected Zones in Cast Precipitation-Hardened Stainless Steels 17-4 and 13-8+Mo

ROBERT J. HAMLIN and JOHN N. DUPONT

Cast precipitation-hardened (PH) stainless steels 17-4 and 13-8 + Mo are used in applications that require a combination of high strength and moderate corrosion resistance. Many such applications require fabrication and/or casting repair by fusion welding. The purpose of this work is to develop an understanding of microstructural evolution and resultant mechanical properties of these materials when subjected to weld thermal cycles. Samples of each material were subjected to heat-affected zone (HAZ) thermal cycles in the solution-treated and aged condition (S-A-W condition) and solution-treated condition with a postweld thermal cycle age (S-W-A condition). Dilatometry was used to establish the onset of various phase transformation temperatures. Light optical microscopy (LOM), scanning electron microscopy (SEM), and energy dispersive spectrometry (EDS) were used to characterize the microstructures, and comparisons were made to gas metal arc welds that were heat treated in the same conditions. Tensile testing was also performed. MatCalc thermodynamic and kinetic modeling software was used to predict the evolution of copper (Cu)-rich body center cubic precipitates in 17-4 and β-NiAl precipitates in 13-8 + Mo. The yield strength was lower in the simulated HAZ samples of both materials prepared in the S-A-W condition when compared to their respective base metals. Samples prepared in the S-W-A condition had higher and more uniform yield strengths for both materials. Significant changes were observed in the matrix microstructure of various HAZ regions depending on the peak temperature, and these microstructural changes were interpreted with the aid of dilatometry results, LOM, SEM, and EDS. Despite these significant changes to the matrix microstructure, the changes in mechanical properties appear to be governed primarily by the precipitation behavior. The decrease in strength in the HAZ samples prepared in the S-A-W condition was attributed to the dissolution of precipitates, which was supported by the MatCalc modeling results. MatCalc modeling results for samples in the S-W-A condition predicted uniform size of precipitates across all regions of the HAZ, and these predictions were supported by the observed trends in mechanical properties. Cross-weld tensile tests performed on GMA welds showed the same trends in mechanical behavior as the simulated HAZ samples. Welding in the S-W-A condition resulted in over 90 pct retention in yield strength when compared to base metal strengths. These findings indicate that welding these PH stainless steels in the solution-treated condition and using a postweld age will provide better and more uniform mechanical properties in the HAZ that are more consistent with the base metal properties.

DOI: 10.1007/s11661-016-3851-6

I. INTRODUCTION

MARTENSITIC precipitation-hardened (PH) stainless steels 17-4 and 13-8 + Mo have been used for a number of applications in the aerospace, nuclear, and military industries due to their high strength, corrosion resistance, and relatively good ductility.[1,2] Both of these materials solidify as δ-ferrite, transform almost entirely to austenite upon cooling, and finally to martensite upon further cooling. The matrix microstructures, therefore, consist of martensite with approximately 10 to 20 pct remnant δ-ferrite and less than a few percent retained austenite.[3–6] The typical heat treatment for these alloys consists of a homogenization step to reverse microsegregation from casting, followed by a solution treatment and quench to produce martensite that is supersaturated, and a final aging step. The aging step is typically conducted at temperatures between 723 K and 923 K (450 °C and 620 °C) for 1 to 5 hours to promote the formation of fine nanometer-scale precipitates. Alloy 13-8 + Mo is strengthened by β-NiAl precipitates and 17-4 is strengthened by BCC copper (Cu)-rich precipitates.[6] The evolution of the matrix

ROBERT J. HAMLIN, Research Assistant, and JOHN N. DUPONT, Professor, are with the Department of Materials Science and Engineering, Lehigh University, Bethlehem, PA 18015. Contact e-mail: rjh212@lehigh.edu
Manuscript submitted May 27, 2016.
Article published online November 2, 2016

microstructure and precipitates through the HAZ will determine the final mechanical properties. Therefore, it is necessary to understand the evolution of phase transformations within the matrix microstructure during heating and cooling as well as potential changes to the morphology of precipitates.

Dilatometry experiments were performed at various heating rates for PH 17-4 and 13-8 + Mo by Kapoor *et al*. to identify precipitation temperatures of these alloys.[7] It was determined that precipitation begins at temperatures between 673 K and 823 K (400 °C and 550 °C) for both 17-4 and 13-8 + Mo and ends at temperatures between 773 K and 873 K (500 °C and 600 °C), depending on the heating rate. It was also observed that the martensite to austenite transformation began at temperatures between 923 K and 1173 K (650 °C and 900 °C) and finished at temperatures between 1023 K and 1223 K (750 °C and 950 °C), depending on heating rate.[7] These findings suggested that significant microstructural changes can be expected in the HAZ of these alloys during welding.

MatCalc thermodynamic and kinetic modeling software is a useful tool that can be used to predict the evolution of the precipitates in these materials as they are subjected to weld thermal cycles. In the work performed by Povoden-Karadeniz and Kozeschnik,[8] the modeling of β-NiAl precipitates in PH 13-8 + Mo was investigated. The mean radius, number density, and phase fraction of β-NiAl were calculated as a function of aging time at 848 K (575 °C). It was determined that the critical precipitate radius, after which strength in the material decreased, was 3.8 nm. These findings compared well with experimental data acquired using TEM and 3D atom probe.[8] Similar modeling studies performed by Holzer and Kozeschnik[9] calculated the mean radius, number density, and phase fraction of copper precipitates in iron-copper systems aged at 773 K (500 °C). The results of that work demonstrated that the precipitates consist of the BCC structure for approximately 8 hours, after which the average size exceeds 4 nm and the precipitates transform to the FCC structure. These predicted trends were consistent with observations found in the literature.[9,10]

The temperatures experienced in the HAZ of fusion welds are high enough to result in coarsening and dissolution of precipitates. Thus, these alloys are often welded in the solution-treated condition and then given a postweld aging treatment to promote precipitation throughout the base metal, HAZ, and fusion zone (FZ) simultaneously.[6] However, when welding on a large scale or making a repair weld it may be necessary to weld in the aged condition. Thus, it is important to understand how the properties of these materials change when welded in different conditions. Experiments were performed by Bhaduri *et al*.[1] on the welding and postweld heat treatment (PWHT) of PH 17-4 welded in the solution-treated and aged conditions using different heat inputs for GTAW and shielded metal arc welding (SMAW). It was found that welding in the solution-treated condition resulted in higher and more uniform hardness across the base metal, HAZ, and FZ, than welding in the aged condition. The observed trends in mechanical properties were attributed to the dissolution and coarsening of Cu precipitates as well as tempering of the martensitic matrix.[1]

Many applications involving these materials will require joining, making it necessary to understand how the microstructure and mechanical properties of these materials will respond to processes such as fusion welding. In this work, 13-8 + Mo and 17-4 in the solution-treated or aged condition were subjected to thermal cycles and peak temperatures characteristic of different regions in the HAZ for fusion welding. Dilatometry, light optical microscopy (LOM), scanning electron microscopy (SEM), and energy dispersive spectrometry (EDS) were used to characterize the microstructures, and MatCalc was used to predict how the precipitates were expected to evolve through the HAZ. The microstructural findings and modeling results were then compared to the tensile properties and hardness measurements for each region of the HAZ for both materials. Comparisons were then made between the tensile property results for the simulated HAZ samples and the GMA welds.

II. EXPERIMENTAL

The chemical compositions of the PH 17-4 and PH 13-8 + Mo alloys and filler metals used in this study are given in Table I. Two heats were needed to conduct the full range of experiments. Heat 1 was used for the simulations performed on aged materials and Heat 2 was used for simulations on solution-treated material and the GMA welds. The aluminum (Al) concentration was low in the 13-8 + Mo Heat 2 relative to Heat 1, but did not result in a significant change of base metal properties.

Samples were prepared in the aged condition and the solution-treated condition. 17-4 and 13-8 + Mo samples were hot isostatic pressed (HIPed) at 1435 K (1162 °C) and 103 MPa for 4 hours to eliminate porosity and reverse segregation from casting, after which they were air cooled to room temperature. Solution treatment was performed for one hour at 1325 K and 1199 K (1052 °C and 926 °C) for 17-4 and 13-8 + Mo, respectively, followed by an air cool below 305 K (32 °C) for 17-4 and an argon gas cool followed by a water cool below 288 K (15 °C) for 13-8 + Mo. Some samples of 17-4 and 13-8 + Mo were then aged for one and a half hours at 852 K (579 °C) and 4 hours at 866 K (593 °C), respectively.

A Gleeble 3500 thermo-mechanical simulator was used in combination with a quartz rod piezometric dilatometer to perform dilatometry on samples of each material that were 6 mm in diameter and 70 mm long. These experiments were used to determine austenite and ferrite transformation temperatures, which were then used to choose peak temperatures for four regions of the HAZ in each material. Peak temperatures of 923 K, 1148 K, 1423 K, and 1573 K (650 °C, 875 °C, 1150 °C, and 1300 °C) were used for 17-4; and 923 K, 1123 K, 1423 K, and 1573 K (650 °C, 850 °C, 1150 °C, and 1300 °C) were used for 13-8 + Mo. All samples were

Table I. Chemical Composition of PH 17-4 and PH 13-8 + Mo Used in this Study

	Fe	Cr	Ni	C	Mn	Cu	Mo	Al	Si	P	S	Nb
17-4 (heat 1)	bal.	16.24	3.96	0.03	0.49	3.00	0.11	0.00	0.75	0.02	0.01	0.20
13-8 + Mo (heat 1)	bal.	12.70	7.87	0.03	0.16	0.05	2.23	1.14	0.21	0.01	0.01	0.00
17-4 (heat 2)	bal.	16.08	4.09	0.03	0.41	3.02	0.21	0.00	0.83	0.03	0.02	0.20
13-8 + Mo (heat 2)	bal.	12.71	7.90	0.06	0.19	0.13	2.27	0.77	0.22	0.01	0.03	0.00
17-4 filler metal	bal.	16.32	4.70	0.02	0.52	3.54	0.10	0.00	0.51	0.01	<0.01	0.23
13-8 + Mo filler metal	bal.	12.68	8.22	0.04	0.04	0.00	2.12	1.10	0.08	0.01	0.00	0.00

All values are in weight percent.

heated at 20 °C/s. The peak temperatures were used as inputs into the Sandia Optimization and Analysis Routines (SOAR) computer program to calculate thermal cycle cooling rates for each sample that were representative of a heat input of 1500 J/mm.[11,12] The primary objective of this research was to investigate the final microstructure and concomitant properties that result during cooling from various peak temperatures after initial transformation during heating. Initial experiments in this work demonstrated that (as expected) the AC1 and AC3 temperatures were quite sensitive to the heating rate. Thus, to ensure complete transformation during heating, a heating rate of 20 °C/s was used. As shown in Section III, the microstructures and properties obtained using these conditions were representative of the observed microstructures and properties in actual fusion welds on these alloys, verifying the effectiveness of this approach.

Samples of 17-4 and 13-8 + Mo that were in either the aged condition or the solution-treated condition were subjected to each of the thermal cycles. Thermal cycles were performed on 10 mm diameter by 70 mm long rods, which were then machined into samples for tensile tests that were performed to ASTM A370-12a[13] using a modified double-reduced geometry to ensure failure within the targeted region of the HAZ. Samples of 17-4 and 13-8 + Mo, which were in the solution-treated condition prior to the thermal cycles, were aged for one and a half hours at 852 K (579 °C) and 4 hours at 866 K (593 °C), respectively, before mechanical testing was performed. The S-A-W condition refers to samples that were subjected to weld thermal cycles in the solution-treated and aged condition, while the S-W-A condition refers to samples that were subjected to the simulated weld thermal cycles in the solution-treated condition and then given a post-simulation age.

Thermal cycles were also performed on samples of each material which were 6 mm diameter by 70 mm long for characterization. Samples of 17-4 and 13-8 + Mo that were subjected to each thermal cycle in both conditions were prepared using standard metallographic procedures with a final polishing step of 0.05 μm colloidal silica. All samples were etched using a tint etchant consisting of 100 mL stock solution of 5 parts water and 1 part hydrochloric acid with one gram of potassium metabisulfite and 2 g ammonium biflouride. An electrolytic etchant was also applied using 20 g NaOH and 100 mL of water to reveal the presence of δ-ferrite according to etchant 220 of ASTM E407.[14] Etchant 220 is known to stain δ-ferrite and leave martensite and austenite unaffected, making it possible to distinguish the ferrite from the surrounding martensite. Microstructures were characterized using a Reichert Jung MeF3 light optical microscope and a Hitachi 4300 SE/N scanning electron microscope with an X-ray detector for EDS.

Multi-pass GMA welds were made on samples of both materials using matching filler metal, a 200 to 250 A current, 30 to 40 V voltage, 5 mm/s travel speed, and a 393 K (120 °C) preheat and inter-pass temperature. Argon shielding gas was used for the 17-4 GMA welds and 75 pct argon 25 pct helium was used for the 13-8 + Mo GMA welds. Welds were prepared in the S-A-W condition and the S-W-A condition. Welds prepared in the solution-treated condition were given a postweld age of 4 hours at 866 K (593 °C) for 13-8 + Mo and one and a half hours at 852 K (579 °C) for 17-4. Cross-weld tensile tests were performed on each GMA weld according to ASTM A370-12a.[13]

MatCalc thermodynamic and kinetic modeling software was used to model the behavior of the Cu-rich precipitates in 17-4 and of the β-NiAl precipitates in 13-8 + Mo. The phase fraction, number density, and mean radius of precipitates were modeled as a function of time for both systems as they were exposed to each of the HAZ thermal cycles. Thermal cycles were simulated before and after the aging treatments so a direct comparison could be made between the modeling results and the HAZ mechanical properties.

III. RESULTS AND DISCUSSION

A. *Dilatometry*

Dilatometry was performed to determine the transformation start and finish temperatures during the weld thermal cycles for both materials. The dilation curves showing radial expansion as a function of temperature for each region of the HAZ for 17-4 and 13-8 + Mo are shown in Figures 1 and 2, respectively.

The 923 K (650 °C) peak temperature was below the AC1 temperature for both alloys so there was no indication of a phase transformation in the dilation plots, and this HAZ region was termed the subcritical heat-affected zone (SCHAZ). The 1123 K and 1148 K (850 °C and 875 °C) peak temperatures were between AC1 and AC3, and partial austenite transformation was expected on heating. It can be seen in the dilation plots that a phase transformation began at 1070 K and 1006 K (797 °C and 733 °C) for 17-4 and 13-8 + Mo,

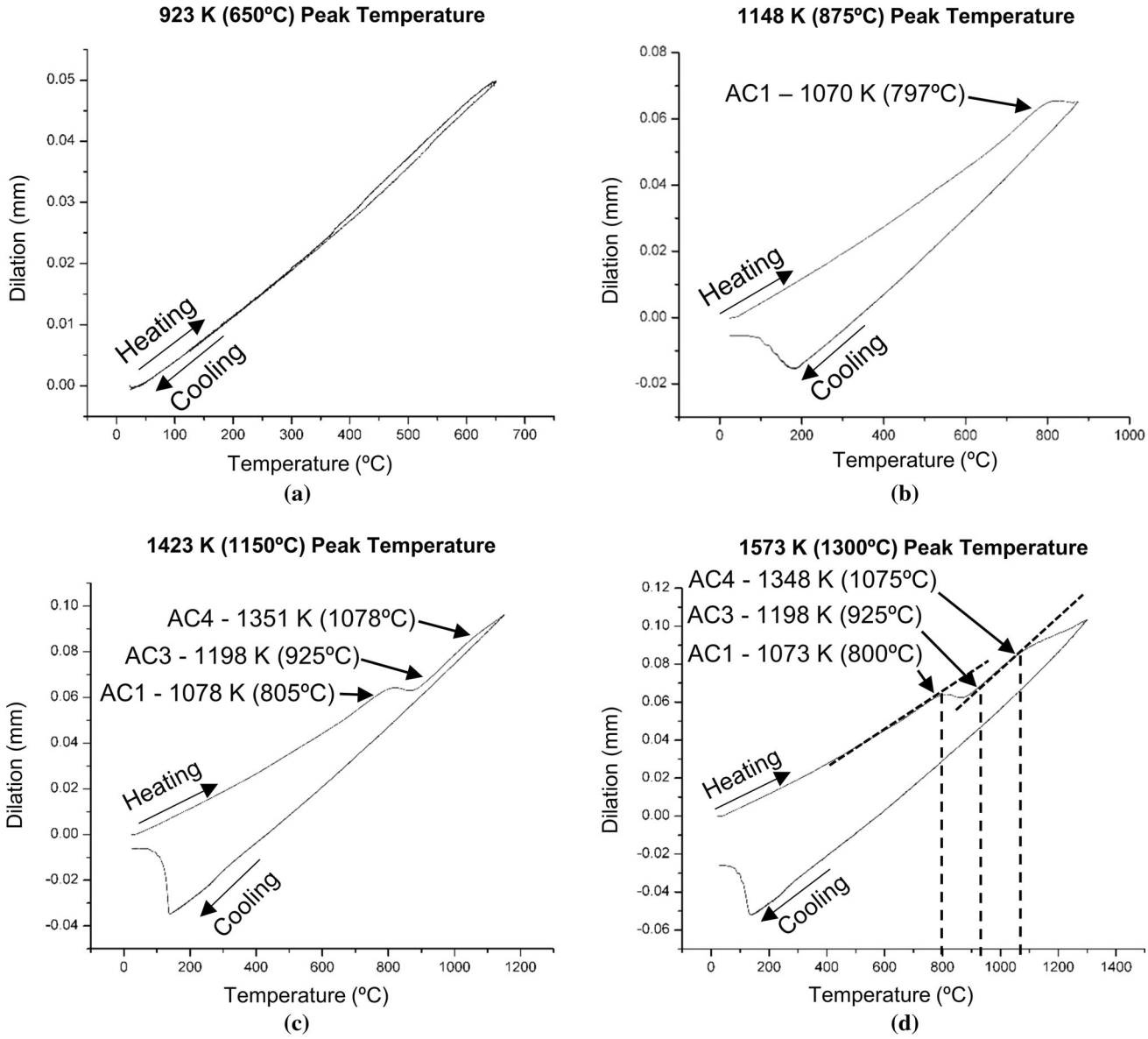

Fig. 1—Dilation as a function of temperature for the (*a*) 923 K (650 °C) peak temperature, (*b*) 1148 K (875 °C) peak temperature, (*c*) 1423 K (1150 °C) peak temperature, and (*d*) 1573 K (1300 °C) peak temperature for PH 17-4 samples subjected to the HAZ thermal cycles.

respectively. However, the transformation at these temperatures was not completed before cooling as indicated by the dilation plots, and this region was labeled the intercritical heat-affected zone (ICHAZ). At a peak temperature of 1423 K (1150 °C), the sample was above AC3 and represented a region where complete austenite transformation was expected on heating. In the dilation plots, on heating a deviation from linear expansion begins and ends at 1078 K and 1198 K (805 °C and 925 °C) for 17-4, and 1003 K and 1170 K (730 °C and 897 °C) for 13-8 + Mo, indicating martensite to austenite transformation start and finish temperatures. Thus, full austenite transformation occurs during heating, which is expected to result in a nearly full as-quenched martensite structure at room temperature. Therefore, this region was labeled the as-quenched martensite heat-affected zone (AQMHAZ). In carbon and low-alloy steels, this HAZ region is referred to as the fine grain HAZ (FGHAZ). However, as explained below, the high-temperature HAZ regions in these alloys are different than carbon and low-alloy steels due to formation of delta ferrite. Thus, an alternate nomenclature is used to reflect this difference. It should be noted that the AQMHAZ peak temperature is above AC4 for 17-4 and below AC4 for 13-8 + Mo. Peak temperatures were initially chosen with respect to AC1 and AC3 for each alloy. The presence of the ferrite transformation was determined later in the investigation and was accounted for in the analysis.

The 1573 K (1300 °C) peak temperature was above the ferrite start (AC4) temperature and increased ferrite formation was expected with increasing temperature. In

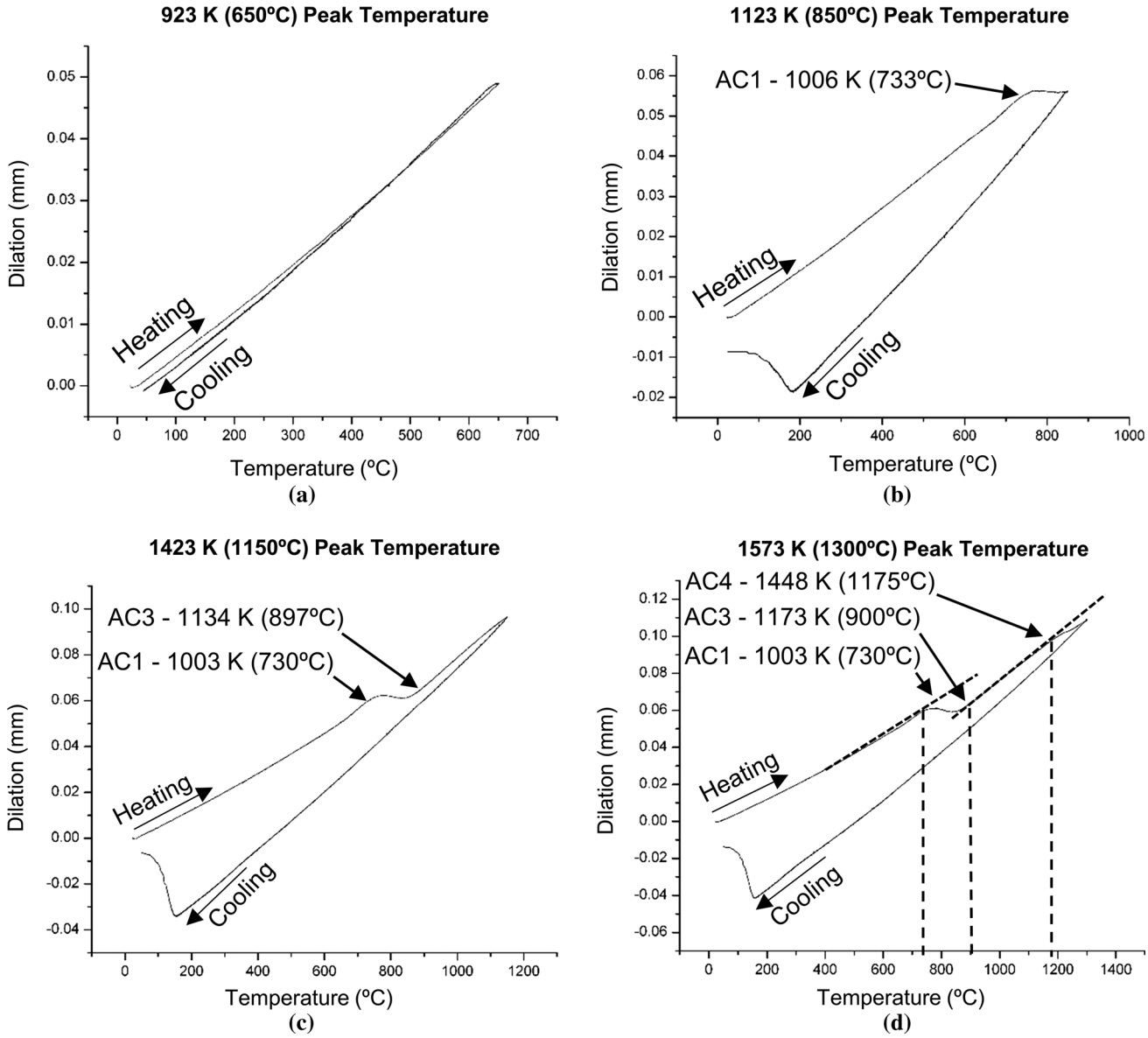

Fig. 2—Dilation as a function of temperature for (*a*) 923 K (650 °C) peak temperature, (*b*) 1123 K (850 °C) peak temperature, (*c*) 1423 K (1150 °C) peak temperature, and (*d*) 1573 K (1300 °C) peak temperature for PH 13-8 + Mo samples subjected to the HAZ thermal cycles.

the dilation plots, a deviation from linear dilation can be seen at 1348 K (1075 °C) for 17-4 and 1448 K (1175 °C) for 13-8 + Mo, indicating δ-ferrite start temperatures. However, the δ-ferrite transformation did not finish. Therefore, this region was labeled the martensite ferrite heat-affected zone (MFHAZ). The measured transformation temperatures are summarized along with the HAZ thermal cycles and precipitate dissolution temperatures (determined using MatCalc) in Figures 3 and 4 for 17-4 and 13-8 + Mo, respectively.

The precipitate dissolution temperatures determined using MatCalc indicate precipitate dissolution could occur within the ICHAZ, AQMHAZ, and MFHAZ for both systems. These results are useful for understanding the types of phase transformations that can occur in each part of the HAZ during the weld thermal cycles.

B. *Microstructural Observations*

The microstructures of the base metals and simulated HAZ samples for 17-4 and 13-8 + Mo prepared in the S-A-W condition are shown in Figures 5 and 6, respectively.

The base metal microstructures consisted of martensite and varying amounts of remnant δ-ferrite. The SCHAZ reached a peak temperature below AC1, so austenite did not form upon heating. Thus, the final microstructures were similar to the base metal, though the martensite experienced additional tempering due to the thermal cycle. The ICHAZ reached peak temperatures above the measured AC1 and below AC3, thus leading to partial austenite transformation during heating. This is consistent with the dilation plots that exhibited a deviation from the local baseline at 1073 K (800 °C) for 17-4 and 1170 K (730 °C) for 13-8 + Mo.

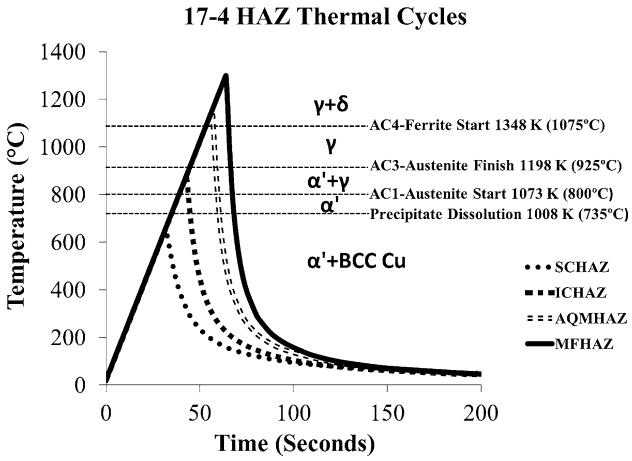

Fig. 3—17-4 HAZ thermal cycles accompanied by transformation temperatures determined using dilatometry and precipitate dissolution temperature (PD) predicted using MatCalc.

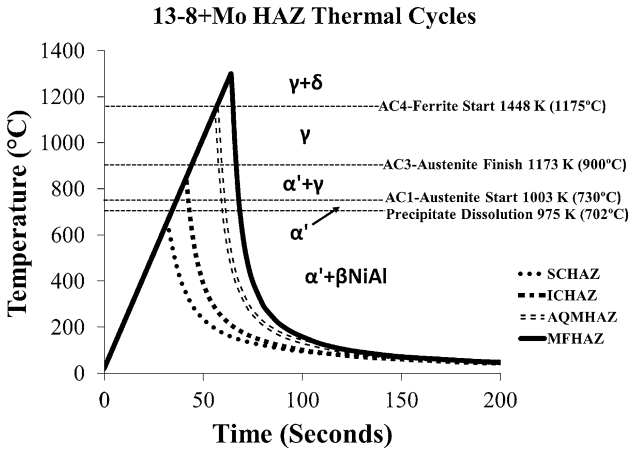

Fig. 4—13-8 + Mo HAZ thermal cycles accompanied by transformation temperatures determined using dilatometry and precipitate dissolution temperature (PD) predicted using MatCalc.

The 17-4 and 13-8 + Mo ICHAZ microstructures had as-quenched martensite along the prior austenite grain boundaries as seen in Figures 5(c) and 6(c), respectively. The as-quenched martensite formed on cooling from the austenite that formed on heating. The AQMHAZ and MFHAZ both experienced temperatures above AC3 and exhibited complete transformation to austenite upon heating. The 17-4 samples show almost complete transformation of austenite in the AQMHAZ and MFHAZ, which is indicated by the dilation plots as well as the photomicrographs in which the matrix consisted primarily of as-quenched martensite. There is also an increase in the amount of δ-ferrite in both regions, which can be seen in the photomicrographs. According to the dilation plots for 17-4, the δ-ferrite start temperature was 1348 K (1075 °C), indicating an increase in the δ-ferrite content should be expected in the AQMHAZ and MFHAZ that experienced peak temperatures of 1423 K and 1573 K (1150 °C and 1300 °C), respectively. As shown at low magnification in Figure 5(d) and in more detail in Figure 7, there was a significant presence of a constituent with a lamellar morphology in the AQMHAZ as well. Low-load microhardness measurements (shown in Figure 7) were taken from the different constituents in the AQMHAZ.

The average δ-ferrite hardness was found to be 243 HV, the as-quenched martensite hardness was found to be 344 HV, and regions that contained the lamellar structure of both phases averaged a hardness of 298 HV. These results suggest that the two-phase lamellar constituent observed in 17-4 could be a mixture of ferrite and as-quenched martensite. (This is confirmed in more detail below.) Dilation plots for 13-8 + Mo indicate full transformation of austenite on heating in both the AQMHAZ and MFHAZ, and the matrix of each microstructure consists of as-quenched martensite. However, the δ-ferrite start temperature for the 13-8 + Mo was 1448 K (1175 °C), which is 373 K (100 °C) higher than the δ-ferrite start temperature of alloy 17-4. There is no change to the δ-ferrite in the AQMHAZ and an increased amount of δ-ferrite in the MFHAZ

Light optical photomicrographs taken from the HAZ of the multi-pass GMA weld made on 17-4 in the S-A-W condition are shown in Figure 8.

The microstructures from the gas metal arc welds (GMAW) HAZ showed good agreement with the microstructures observed in the simulated HAZ samples. The base metal consisted of tempered martensite and δ-ferrite. The SCHAZ appeared similar to the base metal but should be more tempered due to the increased temperatures experienced during the thermal cycle. The ICHAZ consisted of overtempered martensite and small amounts of as-quenched martensite. The AQMHAZ was primarily as-quenched martensite with increased amounts of δ-ferrite. Near the fusion zone, the MFHAZ consisted of as-quenched martensite and large amounts of δ-ferrite. The microstructural trends which have been observed were similar to trends observed in the work performed by Das *et al.*[15] on the weldability of PH 17-4 in the overaged condition. In their work, fusion welds were made on wrought 17-4 in the overaged condition and LOM was used to characterize the microstructures. It was determined that the HAZ consisted of varying amounts of tempered and as-quenched martensite, and that the δ-ferrite content increased with proximity to the fusion zone. Increased amounts of retained austenite were also observed in the higher temperature regions of the HAZ.[15] In other experiments performed by Bhaduri *et al.*,[3] fusion welds were made on samples in the peak-aged condition. It was determined that the martensite evolved through the HAZ in the same manner as was observed in this work; however, no observations were made on the changes to the δ-ferrite morphology.[3]

Light optical photomicrographs taken from the HAZ of autogenous GMA welds made on 13-8 + Mo are shown in Figure 9.

The base metal and SCHAZ consisted of tempered martensite. The ICHAZ contained as-quenched martensite along the prior austenite grain boundaries. The AQMHAZ and MFHAZ consisted almost completely of retransformed martensite and this was consistent with the simulated microstructures. It should be noted that

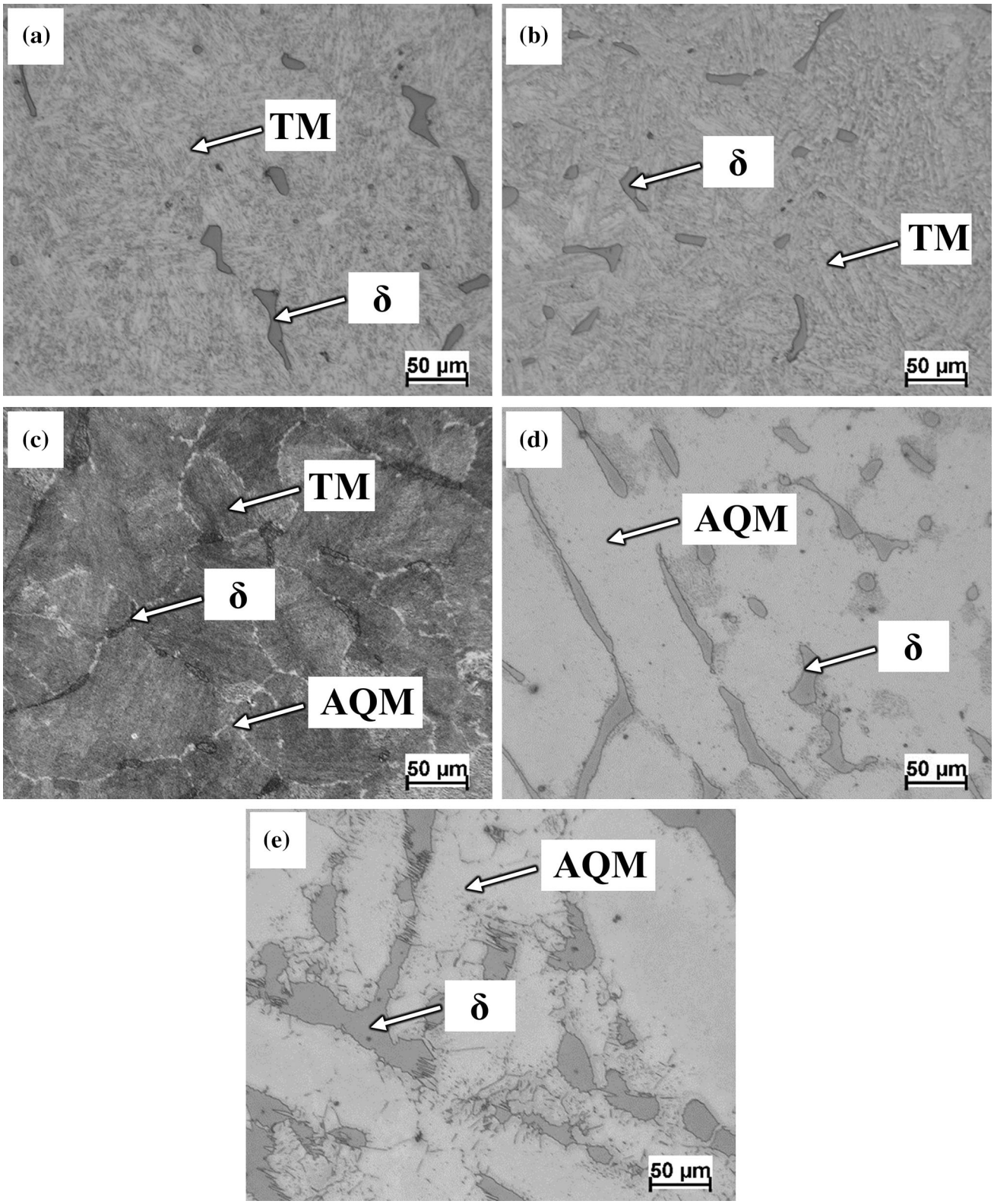

Fig. 5—LOM photomicrographs of 17-4 simulated HAZ samples in the S-A-W condition showing the (*a*) BM, (*b*) SCHAZ, (*c*) ICHAZ, (*d*) AQMHAZ, and (*e*) MFHAZ. TM = Tempered Martensite, AQM = As-Quenched Martensite, δ = δ-ferrite.

there was no significant presence of δ-ferrite in the base metal or any of the GMAW HAZ regions until reaching the MFHAZ. The material used for making the welds was from a different heat than the simulated HAZ samples, so it is possible that the size of the plates and variation in composition lead to the decreased presence

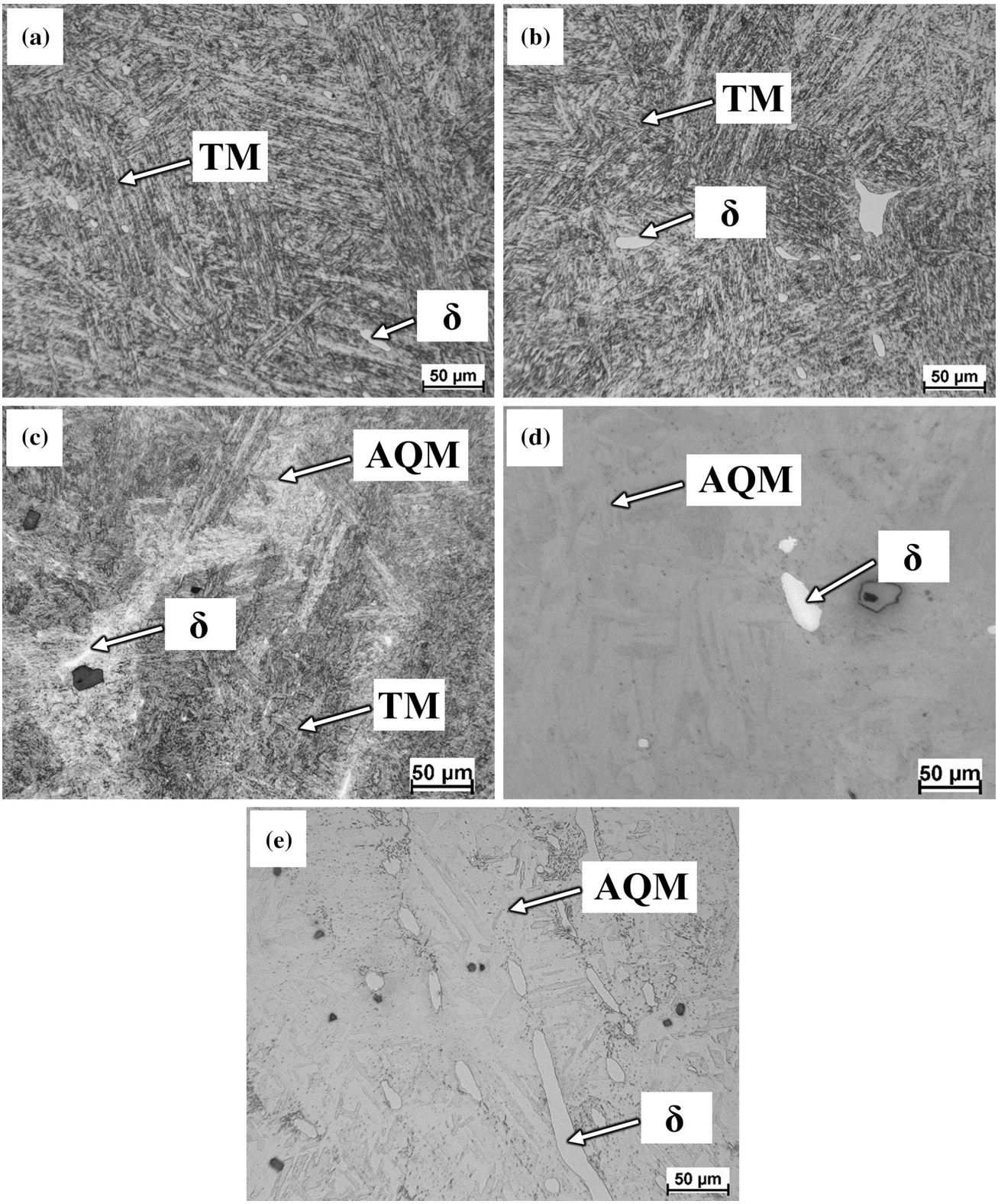

Fig. 6—LOM photomicrographs of 13-8 + Mo simulated HAZ samples in the S-A-W condition showing the (*a*) BM, (*b*) SCHAZ, (*c*) ICHAZ, (*d*) AQMHAZ, and (*e*) MFHAZ. TM = Tempered Martensite, AQM = As-Quenched Martensite, δ = δ-ferrite.

of δ-ferrite. Studies performed by Cieslak *et al.*[16] on the high-temperature solidification behavior of 13-8 + Mo demonstrated that slight changes in composition and slower cooling rates that occur in larger castings could result in a nearly δ-ferrite-free structure.[16] These findings are also supported by the work of Lynch

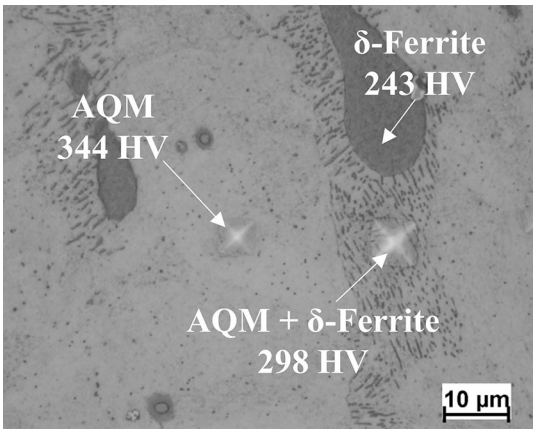

Fig. 7—17-4 S-A-W AQMHAZ showing average hardness values between the AQM, δ-ferrite, and mixed AQM and δ-ferrite regions.

et al.[17] in a heat treat study on cast PH 13-8 + Mo. It was observed that longer times at high temperature resulted in a decrease in the δ-ferrite content.[17] Further investigation of the processing conditions of the as-received plates is required to explain the discrepancies in δ-ferrite content, though the presence of δ-ferrite did not appear to have a significant effect on the mechanical properties (as discussed below).

The nature of the two-phase lamellar constituent observed in the HAZ was investigated further with varying heating rate experiments. The 17-4 alloy was heated to 1573 K (1300 °C) using 1, 20, and 100 °C/s heating rates and rapid cooling rates, the corresponding microstructures were examined with LOM and SEM/EDS techniques. LOM micrographs of these samples are shown in Figure 10.

The two-phase lamellar constituent forms readily at high heating rates. As the heating rate is reduced, the amount of this constituent decreases while the amount of remnant ferrite increases (*i.e.*, coarsens). This suggests that the dark phase within the lamellar constituent is ferrite that is forming along the martensite interlath boundaries. A high-magnification image showing the ferrite formation along lath boundaries is shown in Figure 11.

This ferrite dissolves at slower heating rates (increased time), while the existing remnant ferrite coarsens. To confirm this, EDS was used to measure the composition of each phase, and ThermoCalc was used to estimate the expected composition of ferrite and austenite at 1573 K (1300 °C) (since the austenite will transform to martensite on cooling). The EDS measurements were acquired on the sample heated at 1 °C/s, since this provided large phases that were bigger than the interaction volume of the electron beam (~1 μm^3). The EDS measurements and ThermoCalc compositions are provided in Table II, which are averages of at least five measurements made on each phase. The compositions provided by ThermoCalc for ferrite and austenite match very closely with the EDS measurements. In addition, the results show the expected trend in which the martensite [austenite at 1573 K (1300 °C)] was enriched with Ni and Cu, while the ferrite was enriched with Cr. These results indicate that the lamellar constituent in the HAZ is indeed martensite and δ-ferrite. Ferrite formation along lath boundaries was also observed by Wu and Lin[18] during a study on the influence of high-temperature exposure on 17-4. Samples were heated to temperatures between 473 K and 673 K (200 °C and 400 °C) for prolonged periods of time. It was determined using TEM and selected area diffraction (SAD) that recrystallized α-ferrite formed along the martensite laths during the aging treatments giving rise to the lamellar-like structure.[18] The preferential formation of δ ferrite in these locations indicates an enrichment of ferrite-stabilizing elements. Thermodynamic and kinetic modeling calculations were performed by Babu *et al.*[19] to predict phase stability in various materials during heat treatment. Results of that work showed that small concentration gradients were enough to stabilize Ferrite in PH 17-4 stainless steel when exposed to temperatures in the δ-ferrite + Austenite phase region.[19] Ferrite and Austenite are stable at these temperatures, thus minor changes in concentration are sufficient to stabilize one phase over the other. The results showed that these phases could be stabilized down to room temperature.[19]

The aging treatment applied to the S-W-A samples had no significant effect on the matrix microstructure. Light optical photomicrographs of the 17-4 and 13-8 + Mo samples prepared in the S-W-A condition are shown in Figures 12 and 13, respectively.

The evolution of the δ-ferrite remained the same, but the as-quenched martensite that formed during the HAZ thermal cycles was tempered due to the aging treatment, and the martensite which was tempered prior to aging was further tempered. A 20 g NaOH, 100 mL water electrolytic etch was applied to the 13-8 + Mo MFHAZ sample to help resolve the δ-ferrite, and a photomicrograph of the same region at a higher magnification is shown in Figure 13(f). The dark constituent is ferrite that was stained by the etchant, while the surrounding martensite was unaffected.

C. *Mechanical Properties*

The tensile properties of 17-4 and 13-8 + Mo simulated HAZ samples in the S-A-W and S-W-A conditions are shown in Figures 14 and 15.

Different heats were used for each condition. However, the base metal strength values were consistent between heats, indicating the compositional variations were not significant. The alloys prepared in the S-A-W condition showed decreased yield strength through the HAZ when compared to their respective base metals. Samples prepared in the S-W-A condition possessed higher and more uniform yield strength values through the HAZ for both materials. The tensile strength of both materials in both conditions remained relatively constant through all regions of the HAZ. This indicated that the loss in yield strength was recovered through work hardening before failure. This is consistent with the high ductility (~50 pct RA) observed in all the HAZ regions. Note that the trend observed here, in which the strength increases during aging,

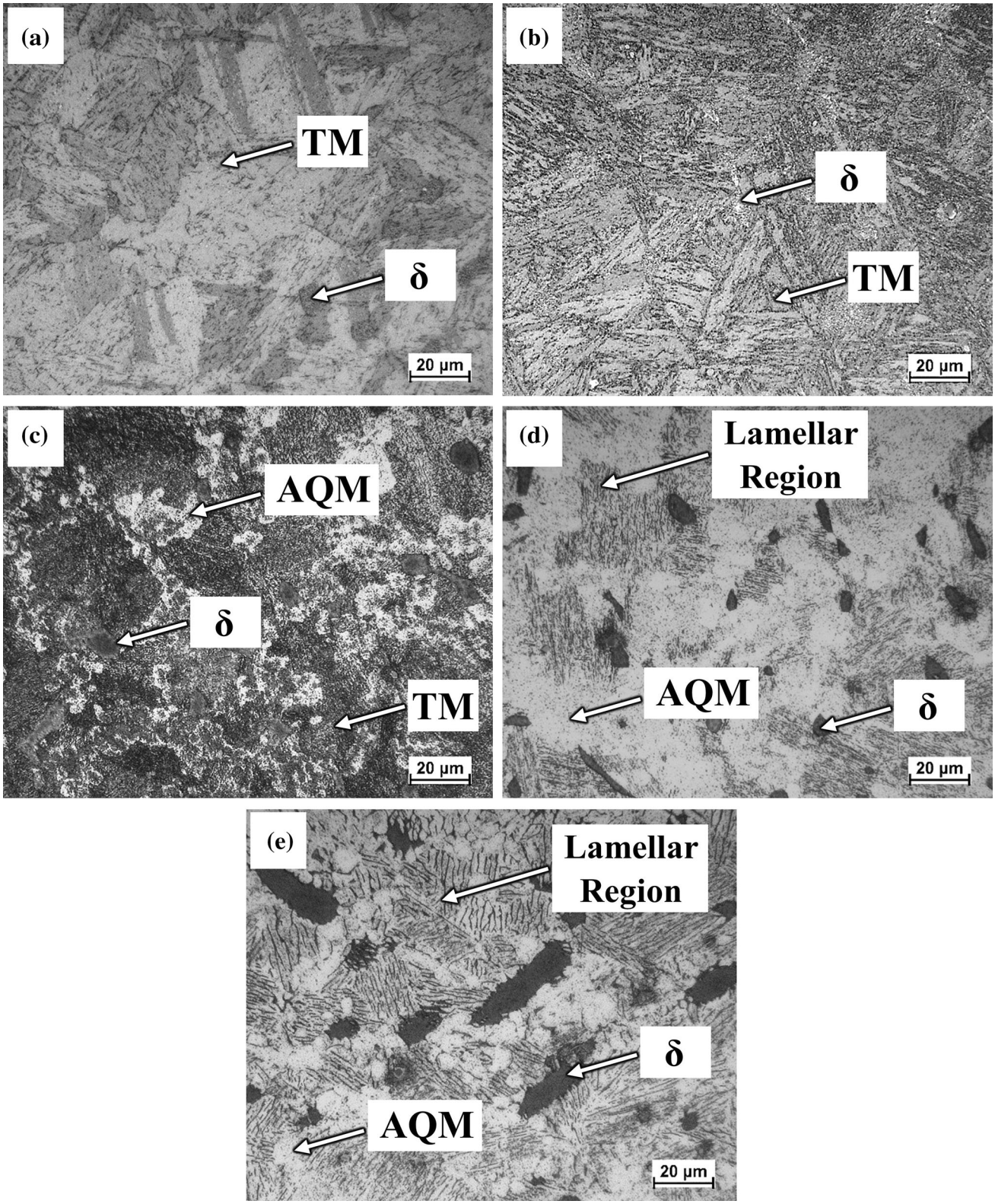

Fig. 8—LOM micrographs of a 17-4 GMA weld in the S-A-W condition taken from (*a*) the base metal, (*b*) SCHAZ, (*c*) ICHAZ, (*d*) AQMHAZ, (*e*) MFHAZ. TM = Tempered Martensite, AQM = As-Quenched Martensite, δ = δ-ferrite.

cannot be associated with tempering of martensite within the matrix microstructure. Typically tempered martensite produces decreased strength when compared to as-quenched martensite.[20] The HAZ samples prepared in the S-W-A condition possessed microstructures that consisted of primarily tempered

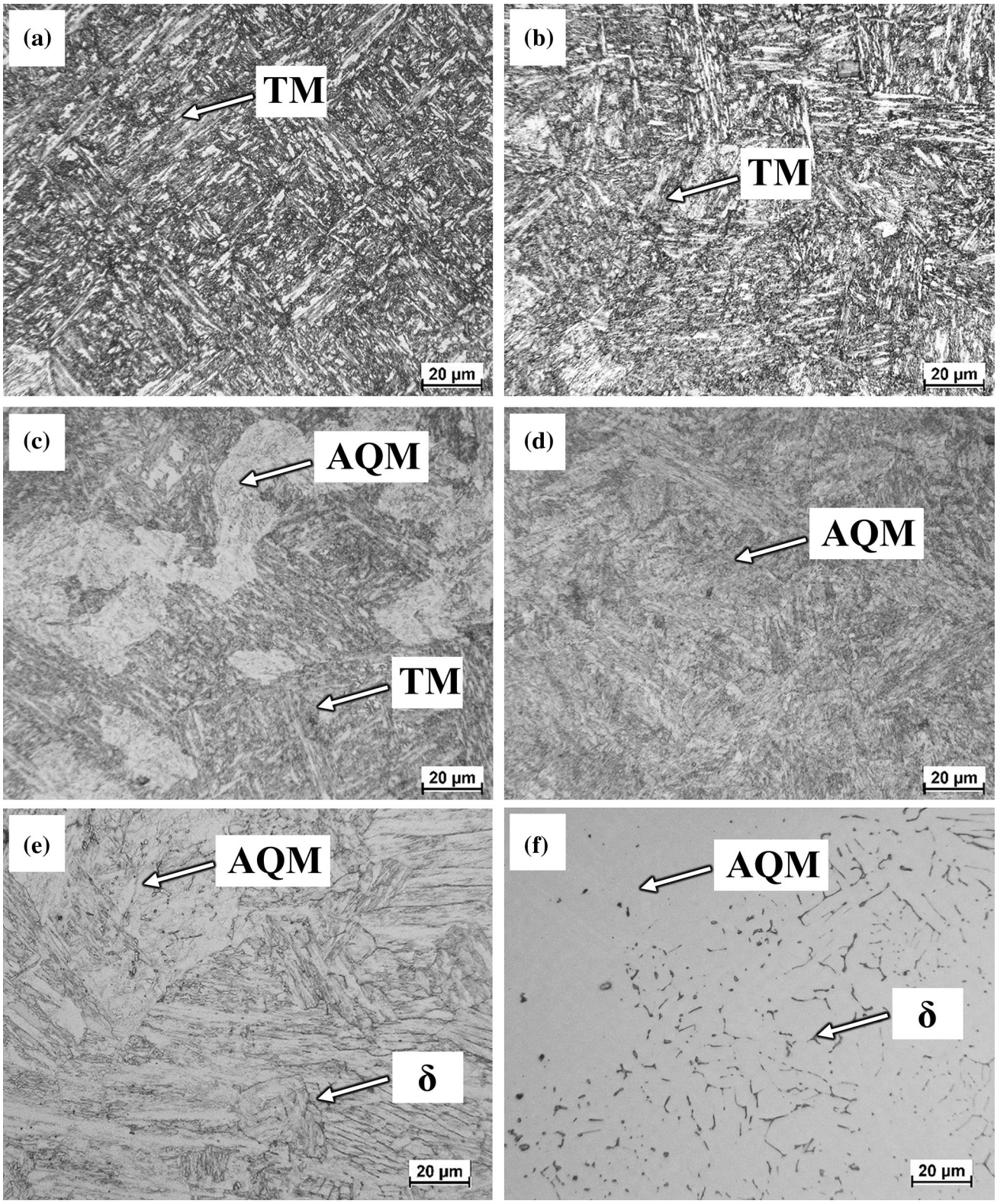

Fig. 9—LOM micrographs of a 13-8 + Mo GMA weld in the S-A-W condition taken from (*a*) the base metal, (*b*) SCHAZ, (*c*) ICHAZ, (*d*) AQMHAZ, (*e*) MFHAZ, and the (*f*) MFHAZ, etched using NaOH to reveal δ-ferrite. TM = Tempered Martensite, AQM = As-Quenched Martensite, δ = δ-ferrite.

martensite and showed higher strength values than samples prepared in the S-A-W condition which contained as-quenched martensite. Thus, the increase in strength associated with the aging treatment can be attributed to reformation of the strengthening precipitates.

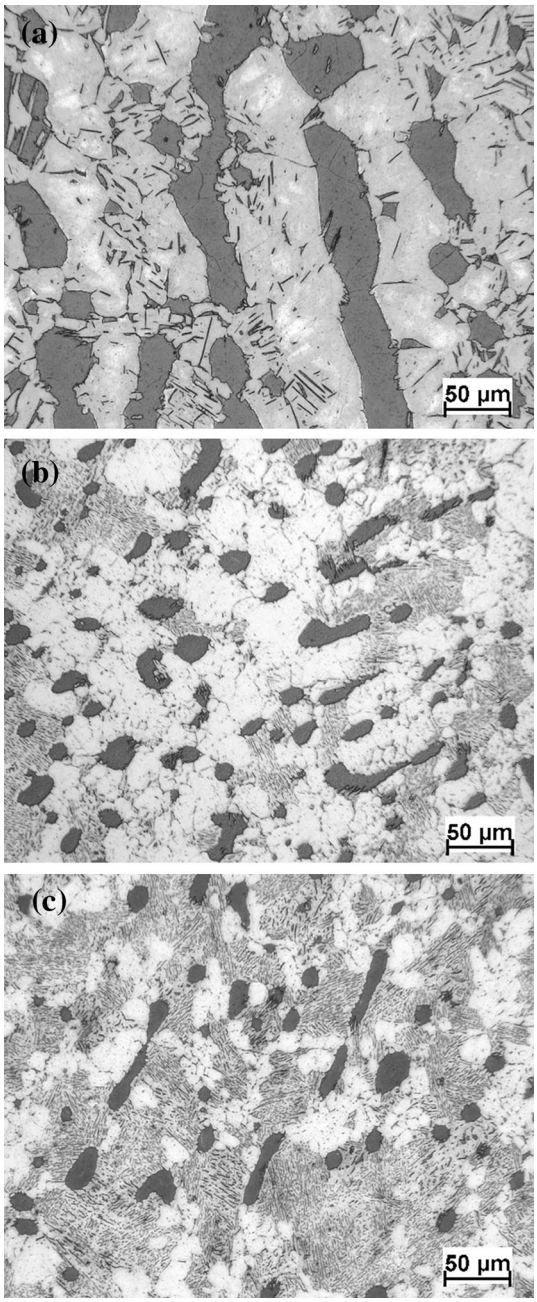

Fig. 10—LOM micrographs of 17-4 samples heated at (*a*) 1 °C/s, (*b*) 20 °C/s, and (*c*) 100 °C/s to 1573 K (1300 °C).

Cross-weld tensile results from GMA welds on both materials are given in Table III. The trends observed in the mechanical properties of the GMAW samples were consistent with the trends observed in the simulated HAZ samples. Samples prepared in the S-W-A condition showed higher tensile and yield strengths than samples prepared in the S-A-W condition. The yield strength values of samples in the S-W-A condition were over 90 pct of their respective base metal values, compared to only 72 and 76 pct for the S-A-W condition.

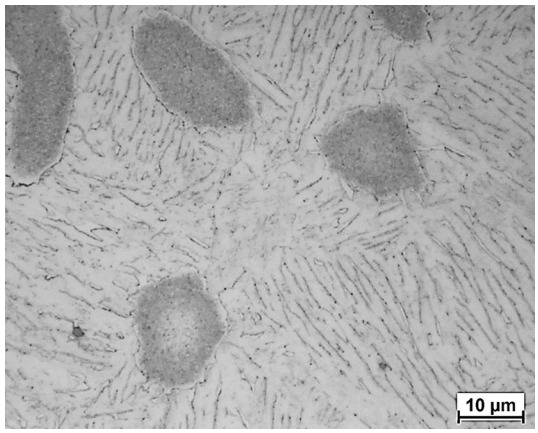

Fig. 11—LOM micrographs of ferrite formation along lath boundaries in the 17-4.

Precipitation-strengthened materials often possess a coarsened zone when welded in the aged condition, and strength cannot typically be restored in this region by subsequent heat treatment. Coarsened regions can also form when welding in the solution-treated condition if a direct age is applied. Exposure to welding thermal cycles can result in precipitation in some regions of the HAZ after which aging can cause precipitate coarsening. However, the mechanical test results from the simulated HAZ samples and full-scale welds show that nearly all the strength can be restored in these materials by subsequent PWHT, which suggests that the coarsened region is not significant in these alloys. Research by Ping *et al.*[21] on β-NiAl precipitates and studies on Cu precipitation in a ferritic steel performed by Bono *et al.*[22] demonstrated that these materials are resistant to coarsening due to segregation of alloying elements to the precipitate/matrix boundary. In these studies, segregation of alloying elements, such as Mo, Ni, and Mn, to the precipitate/matrix interface were observed using atom probe tomography and it was concluded that this segregation created a diffusion barrier, slowing the precipitation kinetics and preventing the effects coarsening.[21,22] This effect carries important practical significance, as it provides the opportunity for a direct age treatment after welding for restoring strength without the need for a prior high-temperature solution treatment.

D. *Modeling Results*

The strengthening in PH stainless steels arises from the hindering of dislocation movement during plastic deformation by fine nanometer-sized precipitates. The peak hardness in 17-4 and 13-8 + Mo arises when the precipitate's size is between 2 and 5 nm for 17-4 and 2-6 nm for 13-8 + Mo, at which point they are coherent with the matrix and the dislocations must shear through them during deformation.[8,21,23] This information can be used to relate trends in the mechanical properties to the phase fraction, mean radius, and number density of precipitates in these materials.

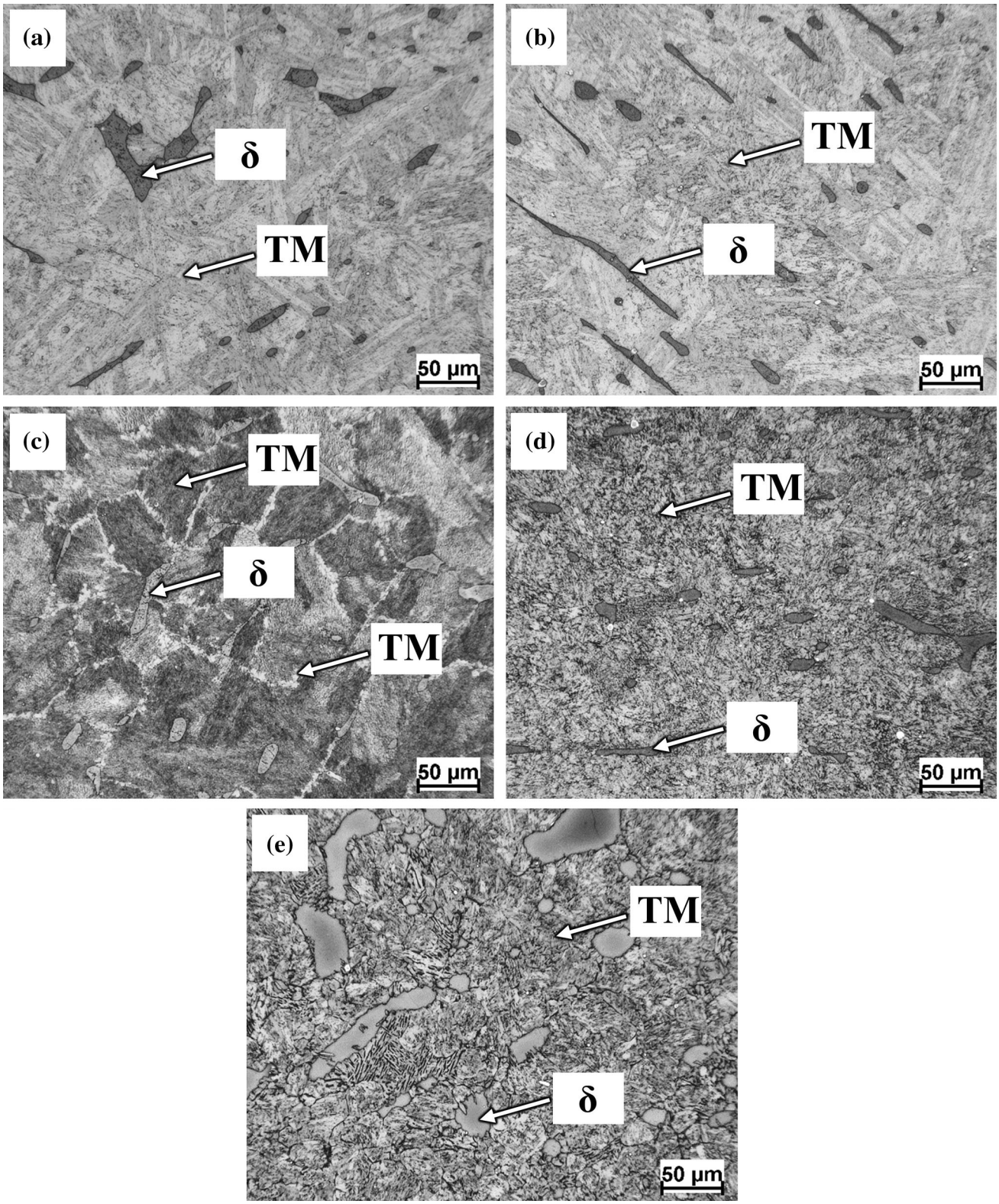

Fig. 12—LOM photomicrographs of 17-4 simulated HAZ samples in the S-W-A condition showing the (*a*) BM, (*b*) SCHAZ, (*c*) ICHAZ, (*d*) AQMHAZ, and (*e*) MFHAZ. TM = Tempered Martensite, δ = δ-ferrite.

The MatCalc results showing the thermal cycle accompanied by the phase fraction, mean radius, and number density of BCC Cu-rich precipitates for the MFHAZ of 17-4 are shown in Figure 16 as an example.

The phase fraction, number density, and mean radius drop to zero during the thermal cycle, indicating complete dissolution of the precipitates. The phase fraction was very low for the remainder of the thermal

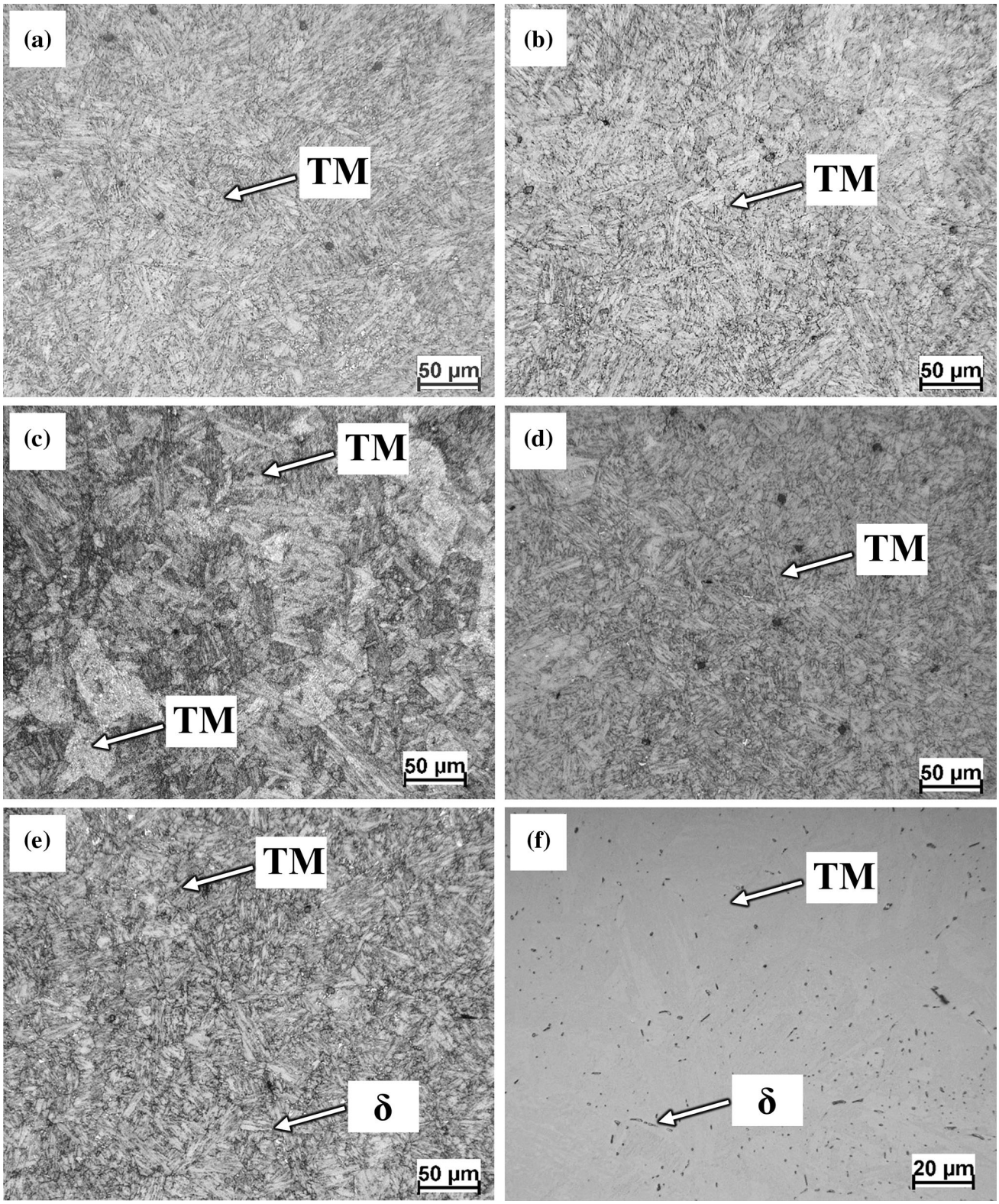

Fig. 13—LOM photomicrographs of 13-8 + Mo simulated HAZ samples in the S-W-A condition showing the (*a*) BM, (*b*) SCHAZ, (*c*) ICHAZ, (*d*) AQMHAZ, and (*e*) MFHAZ (*f*) MFHAZ, etched using NaOH to reveal δ-ferrite. TM = Tempered Martensite, AQM = As-Quenched Martensite, δ = δ-ferrite.

cycle, while the mean radius increases slightly and the number density increases significantly. These observations indicated some minor re-precipitation during the cooling portion of the thermal cycle. The final values of phase fraction, mean radius, and number density were determined using this process for each thermal

Table II. 17-4 EDS Measurements Taken From Ferrite and Martensite in the Lamellar-Like Constituent

Phase Region	Composition (wt pct)				
	Fe	Cr	Ni	Cu	Mo
Lamellar light constituent	75.4	15.9	4.36	3.02	0.48
ThermoCalc austenite (martensite)	75.5	15.5	4.32	3.27	0.19
Lamellar dark constituent	74.8	17.8	3.35	2.64	0.54
ThermoCalc ferrite	74.7	18.9	2.97	1.83	0.29

ThermoCalc compositions predicted for austenite and ferrite at 1573 K (1300 °C).

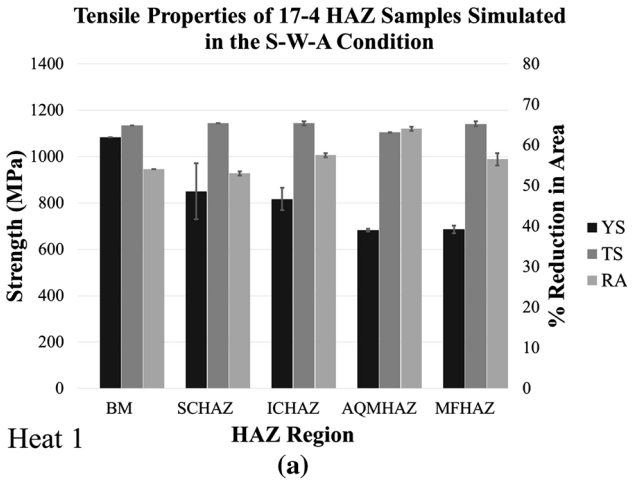

Fig. 14—Tensile properties of the base metal and each region of the HAZ for 17-4 simulated HAZ samples prepared in (*a*) The S-A-W condition and (*b*) The S-W-A condition.

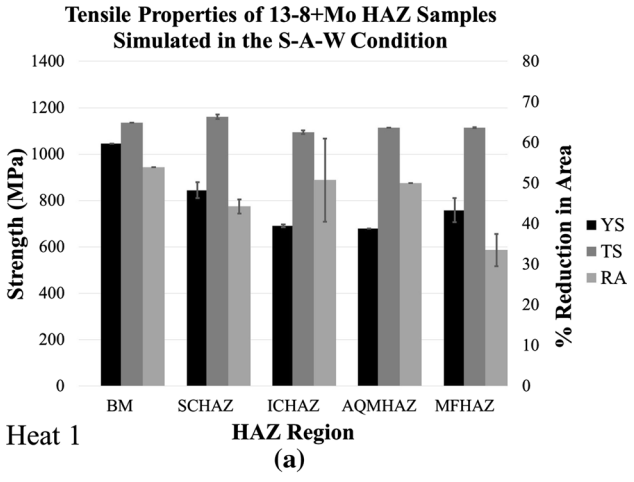

Fig. 15—Tensile properties of the base metal and each region of the HAZ for 13-8 + Mo simulated HAZ samples prepared in (*a*). The S-A-W condition and (*b*) the S-W-A condition.

cycle in both conditions and are summarized in Figure 17.

According to the modeling results for the S-A-W condition, there was relatively no change to the Cu precipitates in SCHAZ for 17-4 when compared to the base metal. Therefore, the decrease in strength observed during the mechanical testing is attributed to additional tempering of the martensitic matrix that occurs during the weld thermal cycle. The ICHAZ experienced a peak temperature above AC1 and below AC3, which would indicate partial austenite transformation on heating. For this condition, the modeling results show a slight decrease in the mean radius size and number density of the Cu precipitates and a rather significant decrease in the phase fraction, indicating partial dissolution. If any partial dissolution of the precipitates occurred within the austenite that formed on heating, it could result in the stabilization of austenite down to room temperature. Using TEM, Viswanathan *et al.*[24] observed the stabilization of austenite down to room temperature due to dissolution of Cu precipitates in PH 17-4 during aging

Table III. Cross-Weld Tensile Results for Multi-pass GMA Welds of 17-4 and 13-8 + Mo

	Yield Strength (MPa)	Tensile Strength (MPa)	Percent of Base Metal Yield Strength Retained
17-4 base metal	1076	1141	N/A
17-4 S-A-W	770	841	72 pct
17-4 S-W-A	1004	1098	94 pct
13-8 + Mo base metal	1092	1181	N/A
13-8 + Mo S-A-W	828	1002	76 pct
13-8 + Mo S-W-A	1016	1165	93 pct

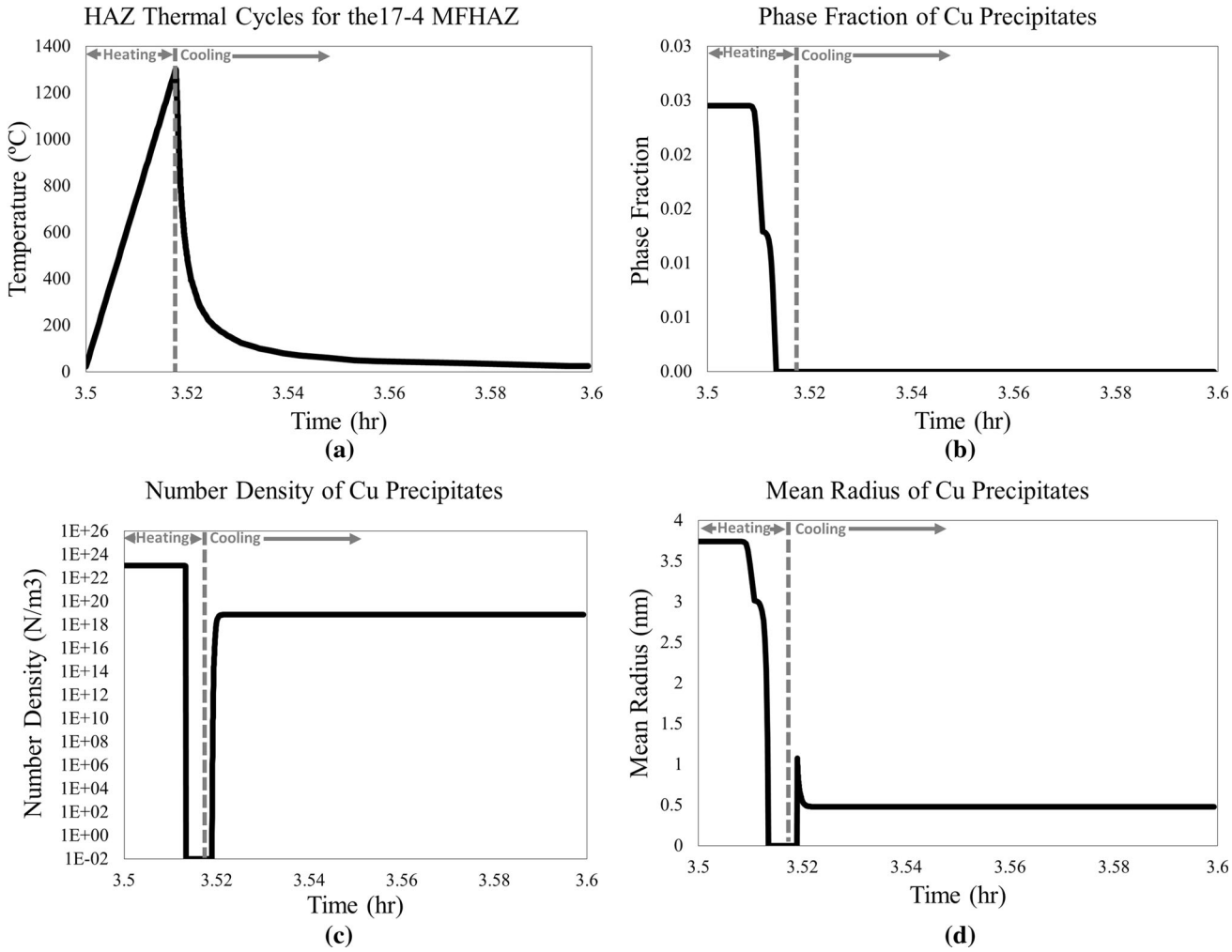

Fig. 16—(*a*) Thermal cycle, (*b*) phase fraction, (*c*) mean radius, and (*d*) number density of Cu precipitates in the MFHAZ of 17-4 simulated in the S-A-W condition, determined using MatCalc.

experiments. This stabilization was attributed to Cu enrichment of the austenite caused by the precipitate dissolution, as copper is an austenite-stabilizing element that, when dissolved in high enough quantities, was believed to suppress the martensite start (M_s) temperature below room temperature.[24] The partial dissolution of the precipitates, coupled with an increase in retained austenite, would explain the decrease in strength observed in this region of the HAZ. The AQMHAZ and MFHAZ both experience temperatures above AC3, resulting in a full austenite transformation on heating. Austenite has a higher solubility than martensite for Cu and with the increased temperatures, complete dissolution of the precipitates was predicted as indicated by the decrease in phase fraction to zero. It should also be noted that on cooling there is some reformation of small precipitates. These precipitates have an average radius of 0.5 nm, which would not be expected to provide a significant increase in strength. According to atom probe tomography results presented by Murthy,[23] the peak hardness was not achieved in samples of 17-4 until the mean radius size was greater than 2 nm.[23] Therefore, the low strength values which were determined in AQMHAZ and MFHAZ are

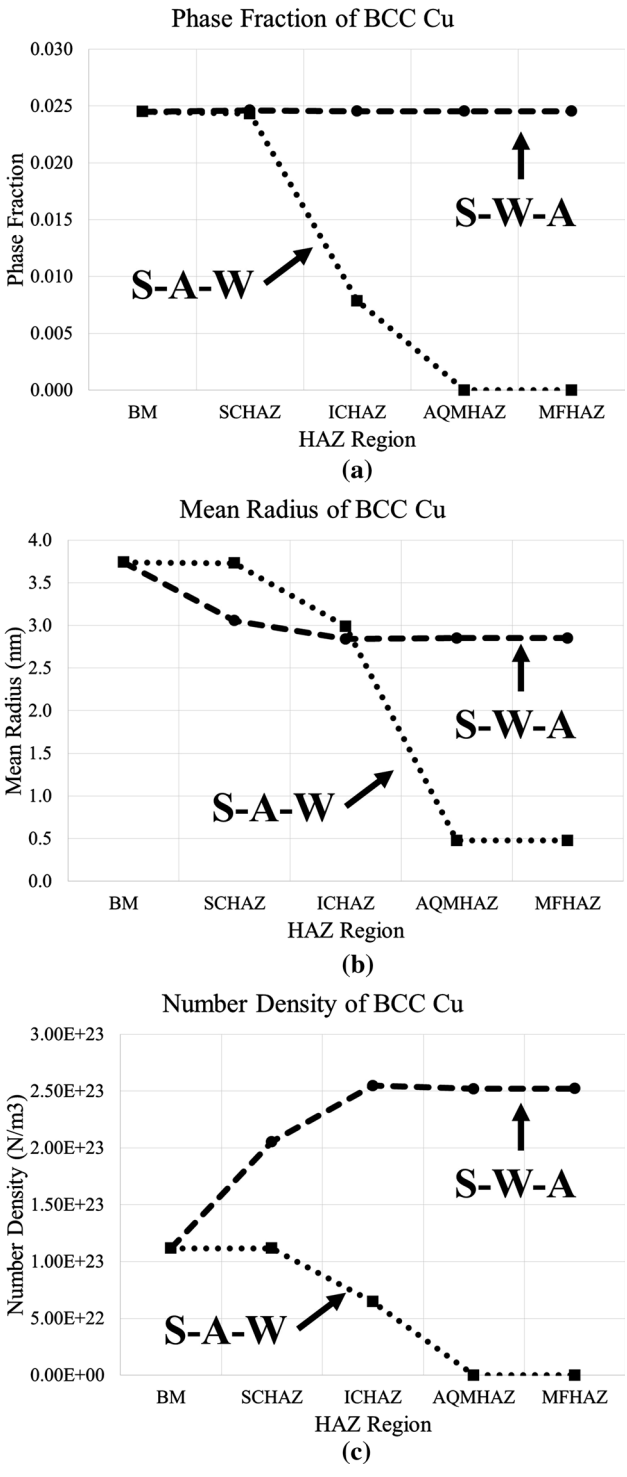

Fig. 17—(*a*) Phase fraction, (*b*) mean radius, and (*c*) number density of Cu precipitates for each region of the HAZ for 17-4 simulated in the S-A-W and S-W-A conditions.

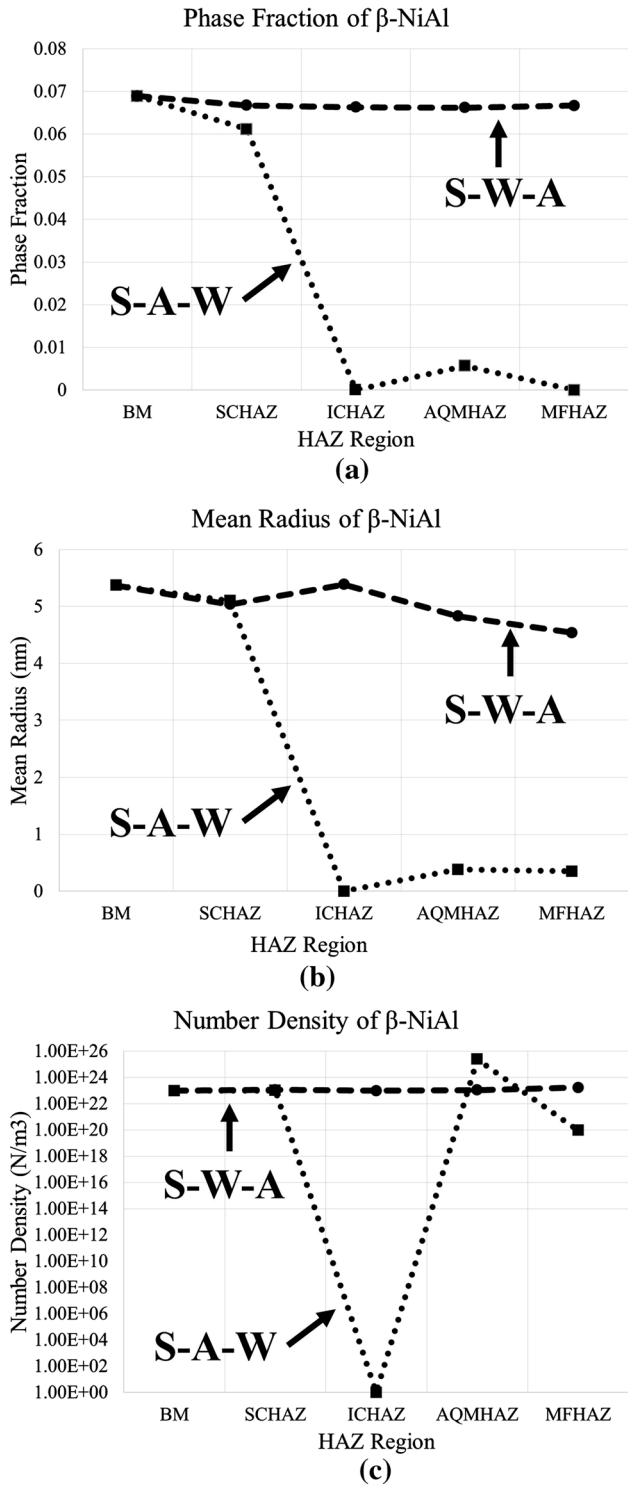

Fig. 18—(*a*) Phase fraction, (*b*) mean radius, and (*c*) number density of *β*-NiAl precipitates for each region of the HAZ for 13-8 + Mo simulated in the S-A-W and S-W-A conditions.

consistent with the nearly complete precipitate dissolution predicted from the modeling results.

The evolution of *β*-NiAl precipitates through the four regions of the HAZ was similar to the Cu-rich precipitate evolution observed in 17-4. The phase fraction, mean radius, and number density of strengthening precipitates in each region of the HAZ of 13-8 + Mo in the S-A-W and S-W-A conditions are shown in Figure 18.

The SCHAZ in the S-A-W condition shows a slight decrease in the number density and phase fraction of *β*-NiAl, which indicates minor dissolution. This slight

dissolution, accompanied by further tempering of the martensite, is consistent with the reduction in strength. The phase fraction, number density, and mean radius are reduced to near zero in the ICHAZ, AQMHAZ, and MFHAZ, and this is also consistent with the decreased strength observed in these three regions. There is some re-precipitation on cooling in AQMHAZ and MFHAZ, but the average radius remains around 0.5 nm and the phase fraction is only about 0.05. Work performed by Ping *et al.*[21] on the characterization of β-NiAl precipitates in a similar 13Cr-8Ni-2.5Mo-2Al stainless steel showed that maximum strength was achieved when precipitates were in the 1 to 5 nm range and 0.01 to 1 vol pct range.[21] Based on these results, the low-phase fraction of very small precipitates expected to form in the ICHAZ, AQMHAZ, and MFHAZ regions would not be expected to significantly contribute to strengthening.

The modeling results for the S-W-A condition show that, for both materials, the final phase fraction, mean radius, and number density are relatively constant through each of the four regions of the HAZ. The uniform size and distribution of precipitates are consistent with the higher and more uniform strength that was measured in the samples tested in the S-W-A condition when compared to samples in the S-A-W condition.

IV. CONCLUSIONS

A study was conducted to determine the effects of welding thermal cycles on the microstructures, mechanical properties, and precipitate evolution of PH 17-4 and PH 13-8 + Mo. HAZ thermal cycles were performed on material in the aged condition and solution-treated condition, after which solution-treated samples were given a post-simulation age. The following conclusions can be drawn from this work:

1. Simulated HAZ and GMAW microstructures in the as-welded condition consisted of tempered martensite in the base metal and SCHAZ, overtempered and as-quenched martensite in the ICHAZ, and primarily as-quenched martensite in the AQMHAZ and MFHAZ. The δ-ferrite content increased in the AQMHAZ and MFHAZ of 17-4 samples and increased in the MFHAZ of the 13-8 + Mo samples.
2. The yield strength was significantly reduced in the 17-4 and 13-8 + Mo HAZ samples prepared in the S-A-W condition when compared to their respective base metals. The loss in strength was attributed to the dissolution of the strengthening precipitates. The tensile strength of HAZ samples for both materials in both conditions remained relatively constant regardless of heat treatment, which was attributed to the high reduction in area values for the samples with low yield strengths, indicating that work hardening was occurring.
3. The 17-4 and 13-8 + Mo HAZ samples prepared in the S-W-A condition had higher and more uniform yield strength when compared to the samples prepared in the S-A-W condition. The improved strength was attributed to the formation and growth of precipitates uniformly in each region of the HAZ for the S-W-A condition
4. Changes observed in the matrix microstructure (*i.e.*, the relative phase balance of martensite, austenite, and ferrite) had a minimal effect on the mechanical properties. Decreased strength in S-A-W samples was attributed to the dissolution of Cu-rich and β-NiAl precipitates through the HAZ of 17-4 and 13-8 + Mo, respectively. The uniform strengths in the S-W-A condition were attributed to precipitate nucleation and growth within each region of the HAZ.
5. Cross-weld tensile testing on GMA samples showed the same trends as the simulated HAZ samples. Strength was higher in the welds prepared in the S-W-A condition when compared to the S-A-W condition. It was also observed that over 90 pct of the base metal yield strength was retained when samples were welded in the S-W-A condition.

ACKNOWLEDGMENTS

The Authors would like to gratefully acknowledge financial support for this research through American Metal Casting's Casting Solutions for Readiness program that is sponsored by the Defense Supply Center Philadelphia, Philadelphia, PA, and the Defense Logistics Agency Research & Development Office, Ft. Belvoir, VA.

REFERENCES

1. A.K. Bhaduri, S. Sujith, G. Srinivasan, T.P.S. Gill, and S.L. Mannan: *Weld. J. (Miami)*, 1995, vol. 74, pp. 153–59.
2. J.A. Brooks and W.M. Garrison, Jr.: *Weld. J. (Miami)*, 1999, vol. 78, pp. 280–91.
3. A.K. Bhaduri and S. Venkadesan: *Steel Res.*, 1989, vol. 60, pp. 509–13.
4. P.W. Hochanadel, G.R. Edwards, C.V. Robino, and M.J. Cieslak: *Metall. Mater. Trans. A*, 1994, vol. 25A, pp. 789–98.
5. P. Wanjara and M. Jahazi: *Can. Metall. Q.*, 2008, vol. 47, pp. 413–36.
6. J.C. Lippold and D.J. Kotecki: *Welding Metallurgy and Weldability of Stainless Steels*, Wiley, Hoboken, 2005, pp. 269–74.
7. R. Kapoor and I.S. Batra: *J. Mater. Sci. Eng. A*, 2004, vol. 371, pp. 324–34.
8. E. Povoden-Karadeniz and E. Kozeschnik: *ISIJ Int.*, 2012, vol. 52, pp. 610–15.
9. I. Holzer and E. Kozeschnik: *Mater. Sci. Forum*, 2010, vols. 638–642, pp. 2579–84.
10. E. Kozeschnik: *Scripta Mater.*, 2008, vol. 59, pp. 1018–21.
11. P.P.W. Fuerschbach, G.R. Eisler, and R.J. Steele: *Trends Weld. Res., Proc. Int. Conf., 5th*. 1999. pp. 488–91.
12. P.W. Feurschbach and G.R. Eisler: *Trends Weld. Res., Proc. Int. Conf., 6th*. 2002. pp. 782–86.
13. A01 Committee: *Test Methods and Definitions for Mechanical Testing of Steel Products*, ASTM International, 2012.
14. E04 Committee: *Practice for Microetching Metals and Alloys*, ASTM International, 2007.
15. C.R. Das, H.C. Dey, G. Srinivasan, S.K. Albert, A.K. Bhaduri, and A. Dasgupta: *Sci. Technol. Weld. Join.*, 2006, vol. 11, pp. 502–08.

16. M.J. Cieslak, C.R. Hills, P.F. Hlava, and S.A. David: *Metall. Mater. Trans. A*, 1990, vol. 21A, pp. 2465–75.
17. P.C. Lynch, R.A. Abrahams, and R.C. Voigt: *SFSA T&O Conference, 65th*. 2011. pp. 1–12.
18. J.-H. Wu and C.-K. Lin: *J. Mater. Sci.*, 2003, vol. 38, pp. 965–71.
19. S.S. Babu, J.M. Vitek, and S.A. David: *Heat Treat., Proc. Conf., 20th*. 2000. vol. 2. pp. 641–47.
20. K. Sindo: *Welding Metallurgy*, Wiley, Hoboken, 2003, pp. 393–410.
21. D.H. Ping, M. Ohnuma, Y. Hirakawa, Y. Kadoya, and K. Hono: *J. Mater. Sci. Eng. A*, 2005, vol. 394, pp. 285–95.
22. J.T. Bono, J.N. DuPont, D. Jain, S.-I. Baik, and D.N. Seidman: *Metall. Mater. Trans. A*, 2015, vol. 46A, pp. 5158–70.
23. A.S. Murthy, J.E. Medvedeva, D. Isheim, S.L. Lekakh, V.L. Richards, and D.C. Van Aken: *Scripta Mater.*, 2012, vol. 66, pp. 943–46.
24. U.K. Viswanathan, S. Banerjee, and R. Krishnan: *Mater. Sci. Eng. A*, 1988, vol. A104, pp. 181–89.